Master of Science Thesis

Computational Studies of Torsional Properties of Single-Walled Carbon Nanotubes

Author:
Manana Koberidze
Supervisor:
Pekka Koskinen

University of Jyväskylä

November 19, 2010

Abstract

Current thesis presents computational studies of the torsional twist in single walled carbon nanotubes (SWCNTs). Since SWCNTs can be viewed as rolled up graphene sheets, our aim is to explain their torsion constants via shear modulus of graphene in pristine, and single- and double vacancy cases. In addition, fundamental energy gap response to torsion is investigated. Calculations of defected structures is computationally expensive as it requires larger simulation cell with large number of atoms. To reduce the cost of computations we take the advantage of chiral symmetry of nanotubes instead of translational one, and faster performance of density-functional tight-binding method compared to other computational methods. Shear modulus calculations show that its value approaches that of graphene for large diameter tubes and is most sensitive to size in case of armchair tubes. Vacancies diminish shear modulus for most of the nanotubes and concentration-induced decrease has linear character regardless of chirality. Studies on direction-dependent shearing of graphene reveals that in the presence of double vacancy shear modulus has the biggest fluctuations from its average value compared to pristine and single vacancy instances. Torsion significantly modifies electronic structure as well - metallic tubes undergo transition to semiconducting state, during which band gap change is linear, peaking and decreasing to zero again for most of the tubes. Results give the ground for assumption that for large diameter tubes the peak values, reached during torsion, converge.

Preface

The work introduced in the thesis was done at the Nanoscience Center, Department of Physics of the University of Jyväskylä during November 2009 - November 2010.

I would like to express my gratitude to my supervisor, Pekka Koskinen for his determined guidance and helpful advises throughout the work.

I would also like to thank Professor Hannu Häkkinen for giving me the opportunity to explore the field of my keen interest. I am grateful to the whole staff of the Department of Physics and Nanoscience Center, especially, to Riitta–Liisa Kuittinen who have been support whenever I needed.

Finally, I would like to thank my family and friends who have been beside me during the hardest times of my life and who have given me the joy of spending memorable times together.

Jyväskylä, November 2010

Manana Koberidze

Contents

Chapter 1

Introduction

Carbon nanotubes, one of the most studied materials today, have been the subject of wide interest for about two decades. The history traces back to the invention of C60 fullerene mass production method in 1990 [58] when aside C60 researchers noticed unknown filamentous structures during fabrication. Nevertheless, they were treated only as unnecessary by-products. No technology would allow investigations on such a small scale at that time. Those spin-offs were first drawn attention and observed by S.Iijima in 1991 using a high-resolution transmission electron microscopy [45] and thus, concentric, seamless tubules with diameters up to a few tens of nanometer - (multi-walled) carbon nanotubes were first discovered. After two years the discovery was followed by another finding – synthesis of single-walled carbon nanotubes (SWCNTs) [46]. Since then the era of carbon nanotubes began. Over the years carbon nanotubes (CNTs) have intrigued scientists with their amazing mechanical, thermal and electrical properties.

However, as one of the most prominent American writers Alice Walker says: *'In nature, nothing is perfect and everything is perfect'*. Defects like torsion, bending, vacancies are unavoidable during the growth of CNTs. Such imperfections affect their mechanical and electrical properties, as a result, performance of the CNT-based nanodevices and nanomaterials must be different from the idealized case and might be either beneficial or adverse. Consequently, it is of paramount importance to learn how defects alter behavior of carbon nanotubes.

The discovery of these unique materials has intensified interest to other carbon nanostructures, particularly to graphene - a single graphite sheet. It was first isolated experimentally in 2004 by Geim and Novoselov [6] - the breakthrough leading to the Nobel Prize award in 2010 [4]. Though it had been investigated for a long time before, it was believed that graphene could not exist as a free-standing crystal and was unable to form curved structures like fullerenes and nanotubes because of instability. Today, graphene is another topic of intense interest in modern nanoscience and its stability is no longer questionable.

Graphene is the basis of all graphitic materials. Hence, another challenge is to find out how defect-related characteristics of CNTs can be predicted based on those of graphene.

1.1 Structures of graphene and single-walled carbon nanotubes

Bonding is the main determiner of nature of any physical system. In addition, at nanoscale, where every single atom matters, material properties are strongly dependent on system size and geometry. In this section we explain bonding and geometrical structures of graphene and SWCNTs.

Bonding

Carbon has four valence orbitals $2s, 2p_x, 2p_y, 2p_z$ out of which s, p_x, p_y orbital interaction, termed as sp^2 hybridization, forms in-plane bonding (σ or occupied) and in-plane untibonding (σ^* or unoccupied) orbitals in a hexagonal lattice of graphene. σ bonds are of covalent nature and are responsible for binding energy, as a result, for the elastic properties of graphene.

p_z, being perpendicular to the graphene plane, is unable to couple with the orbitals that form σ states but interacts with neighboring p_z orbitals ($pp\pi$ interaction) which

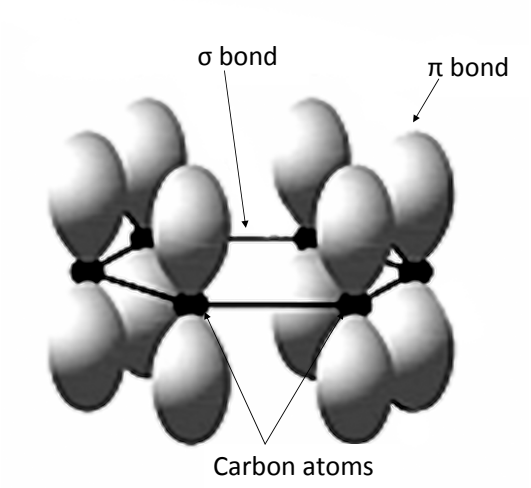

Figure 1.1: σ and π bonding in a hexagonal lattice of graphene. Figure is adopted from reference 2.

establishes delocalized out-of-plane bonding (π) and out-of-plane antibonding (π^*) orbitals. π and σ bonds are illustrated in figure 1.1.

Similarly to graphene, σ bonds provide strong bonding of carbon atoms in a hexagonal manner in CNT wall, whereas π bonds perpendicular to the surface provide weak interaction between SWCNTs in a bundle.

To conclude, the strength of σ bonds are responsible for cohesive energy and elastic moduli of CNTs, whereas π bonds determine their electronic properties.

Geometry

SWCNTs can be viewed as rolled up graphene sheets as shown in figure 1.2. Rolling direction is determined by the *chiral vector*

$$\boldsymbol{C} = n\boldsymbol{a_1} + m\boldsymbol{a_2}, \tag{1.1}$$

which seamlessly connects two crystallographically equivalent sites of graphene forming a tube. $\boldsymbol{a}_1$ and $\boldsymbol{a}_2$ in the above expression represent the unit vectors of the plain honeycomb lattice: $|\boldsymbol{a}_1| = |\boldsymbol{a}_2| = a$. n and m indices give the nomenclature for the three types of nanotubes: armchair $(n, 0)$, zigzag (n, n) and chiral (n, m). Each name refers to the shape of the nanotube edge as depicted in figure 1.3.

The length of the chiral vector defines the circumference of the tube as

$$C = |\boldsymbol{C}| = a\sqrt{n^2 + m^2 + nm}. \tag{1.2}$$

Orientation of the hexagons on the surface of the tube is characterized by *chiral angle* $\theta = \arctan(\sqrt{3}\frac{m}{2n+m})$. It can easily be shown that for armchair tubes $\theta = 30^0$, for zigzag tubes $\theta = 0^0$ and for chiral ones $0 < \theta < 30^0$. Distances between carbon atoms in the hexagonal lattice according to reference 47 are schematically presented in figure 1.4.

The diameter of a SWCNT is on the order of a few nanometers and can be calculated from the following expression:

$$d = \frac{C}{\pi} = \frac{a}{\pi}\sqrt{n^2 + m^2 + nm} \tag{1.3}$$

The length of a CNT can be over 18.5 cm [55], thus, 10^8 times larger than its diameter. Because of such a small diameter-to-length ratio CNTs are considered as one-dimensional structures.

1.2 Properties of carbon nanotubes

Out of plentiful remarkable properties of CNTs, in this section we only discuss electronic and mechanical as the rest are beyond the scope of the current thesis.

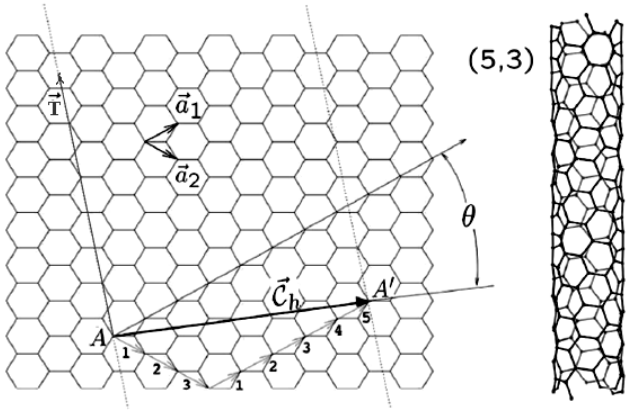

Figure 1.2: Rolling a graphene sheet into a nanotube. Figure is adopted from reference 11.

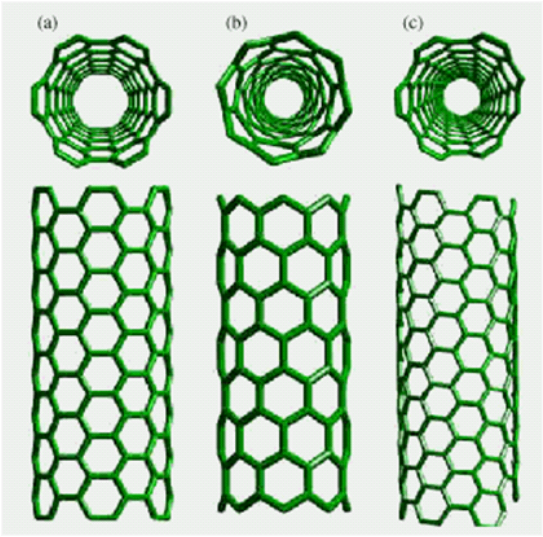

Figure 1.3: The three types of carbon nanotubes: armchair(a), zigzag(b), chiral(c). Figure is taken from reference 5.

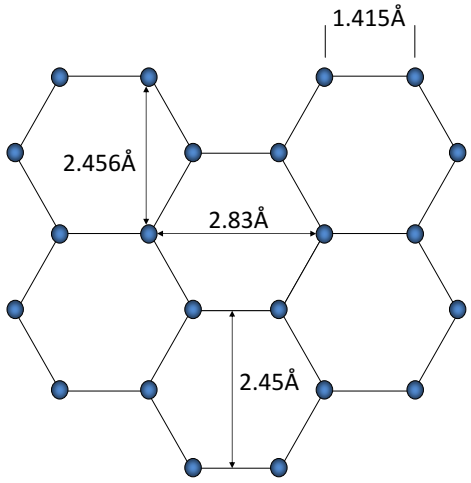

Figure 1.4: Spacing between carbon atoms in graphene lattice according to reference 47.

Electronic Properties

Speaking generally, electronic properties of materials depend on the manner atoms are arranged. An evident manifestation is graphene versus carbon nanotube: although graphene is a zero-gap semiconductor (or, semi-metal) carbon nanotubes can not only be semiconductors with different energy gaps but also metals depending on the rolling direction of the graphene sheet. Based on tight-binding calculations it has been shown that nanotubes for which

$$n - m = 3i, \tag{1.4}$$

where i is an integer, are metallic, otherwise semiconducting [43, 33]. Such correlation between electronic properties of CNTs and their geometry was explained in terms of the band structure of a plane graphene sheet: when rolled in a tube, boundary conditions require that wave-vectors along the tube circumference direction are quantized, *i.e.* only $\boldsymbol{k}$ states fulfilling the condition $\boldsymbol{Ck} = 2\pi q$ are allowed, where q is an integer and $\boldsymbol{C}$ is the chiral vector. These are the lines perpendicular to $\boldsymbol{C}$. Their length, number and orientation with respect to the lattice depend on the chiral indices.

Whether material is metallic or semiconducting is identified with the density of states at Fermi energy. Fermi energy is defined by the K symmetry point which is the meeting point of π and π^* bands of graphene. Nanotube will be metallic if one of the allowed $\boldsymbol{k}$ vectors crosses the K point in the Brillouin zone meaning that there exists finite density of states (no energy gap) at Fermi level. If K point is outside the allowed $\boldsymbol{k}$ vectors then CNTs are semiconducting with varying size of energy gaps. To

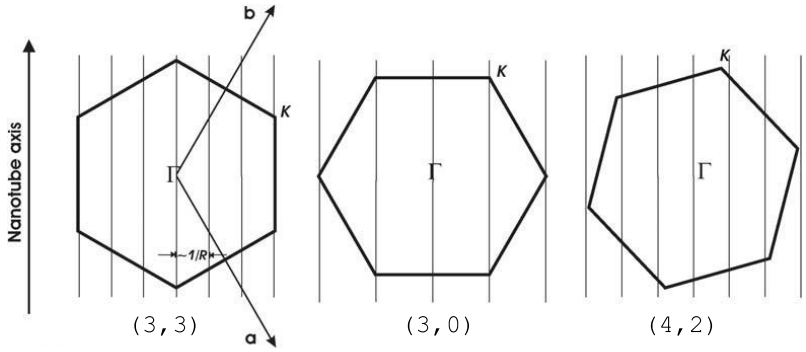

Figure 1.5: Schematics of the first Brillouin zone of a graphene sheet. Lines satisfying condition (1.4) are shown for zigzag (3,3) and armchair (3,0) tubes, indicating at their metallic character. In case of chiral (4,2) tube K point is not crossed by either line meaning semiconductivity of the tube. Figure is adopted form reference [25].

illustrate, allowed $\boldsymbol{k}$ vectors for (3,3), (3,0) and (4,2) nanotubes are shown in figure 1.5.

To mention once more, above discussion is within simple tight-binding model which explains electronic properties of CNTs from the plane graphene and neglects curvature effects. The main purpose of this approximation is to represent the electronic band structure of the nanotube as the superposition of the graphene electronic energy bands along the allowed $\boldsymbol{k}$ vectors, which together with boundary conditions around the tube circumference results in either semiconducting or metallic tubes. Regardless of its simplicity this model works very well for large diameter tubes (above 10 Å) [11]. However, if in graphene in-plane σ and out-of-plane π orbitals are orthogonal and their interaction is excluded, carbon nanotubes represent a structure where carbon atoms are situated on a cylindrical - curved surface, which means possibility of π and σ orbital mixing, especially in small CNTs, where curvature is stronger and more rehybridization occurs. Therefore, more fundamental calculations are needed to predict electronic properties of small diameter CNTs. Even more, in the presence of defects simple tight-binding approach might not be accurate enough since defects significantly modify electronic structure of CNTs.

Mechanical Properties

Carbon nanotubes are one of the most stable materials in nature, at the same time, having light weight and exceptional strength. They are known for their high elasticity, with Young's modulus on the order of 1 TPa [12, 22, 62] and tensile strength of 60 GPa [61]. Various studies have been performed to learn elastic moduli of pristine and deformed CNTs, however, discrepancies in results are yet existent.

Though simple graphene model is often used to describe mechanical properties of CNTs, bending strain caused by curvature in tubes causes an out-of-plane distortion of C-C bonds which results in rehybridization of the sigma bonds as mentioned above. The smaller the diameter of the tube, the higher the bending strain is; and the higher the rehybridization. This means deviating from perfect isotropy present in graphene sheet. Accordingly, mechanical behavior is expected to be dependent on diameter and/or helicity.

It must be underlined that the origin of elasticity is microscopic: despite treating materials as continuous media in classical approach, in fact, elastic properties are governed by the way atoms are bound to each other.

The review of the existing methods and results related to mechanical and electronic properties of SWCNTs under torsion will be presented in Chapter 2.

1.3 Practical applications of CNTs

These unique one-dimensional structures have driven nanoscience towards new technologies and various innovations. Due to their unique mechanical, thermal and electrical properties, CNTs are promising materials for versatile applications in nanoscience:

Because of peculiar electrical characteristics, CNTs can be used as an alternative to the traditional semiconductors in micro-/nano-electronics. Nanotube based transistors are of particular interest. More information on carbon-based nanodevices can be found in reference 36.

Thanks to the tiny size of the ending, CNTs provide single-atom resolution imaging serving as probe tips of Atomic Force Microscopy (AFM). Moreover, their flexibility avoids damaging of the probed surface when scanning, as well as damaging of the tip itself [23].

CNTs are seen as good candidates for flat panel display screens whose performance is based on the phenomenon of electron emission by CNTs in the presence of electric field [53]. Realization of such screens was demonstrated by one of the world's leader companies, Samsung, though their mass production has not been started yet [20].

Several companies have successfully exploited nanocomposites (carbon fibers mixed with nylon) as reinforcing materials, for instance, in hockey sticks [3]. Furthermore, carbon fibers own excellent thermal conductivity that causes nanocomposite materials to cool more slowly and evenly. This ensures better molding on micro scale and are in use for the tiniest gears in watches [18]. More detailed overview of nanocomposites can be found for example, in references 34 and 19.

CNTs are also promising prospects for hydrogen storage elements (hydrogen fuel cells) aimed at development of renewable energy sources: when oxygen and hydrogen interact in a fuel cell, production of electricity is accompanied with water release as byproduct. Therefore, there is demand for a safe, temporary storage for hydrogen

gas. CNTs are expected to be the best choice, as hydrogen atoms form week bonds with carbon, they can easily be expelled by tuning temperature and pressure when needed [13].

Medicine and robotics have benefited from mechanical properties of CNTs as well; and have named them as candidates for artificial muscles. The idea lies in conversion of the electrical energy to mechanical energy causing nanotube to move. Due to their high tensile strength, CNTs would provide about 100 times stronger force than the human muscle of the same size [17, 24].

Besides the above, CNTs are perfect chemical sensors, tiny and fast; in the presence of certain gases (e.g. NO_2, NH_3) semiconducting CNTs exhibit significant change in conductance, this means that by measuring conductance presence of gases can be detected [64].

This is only a short overview to introduce the variety of practical applications and the reasons for such popularity of CNTs not only in academic research but also in industry.

Chapter 2

Previous work on torsional properties of CNTs

Mechanical and electronic properties of distorted carbon nanotubes are still under investigation. Current modeling approaches can be divided into three main categories: atomistic modeling, analytical continuum mechanics and continuum mechanics based on finite element modeling (FEM) [49, 44].

Principal techniques of the first one include classical molecular dynamics (MD), Monte Carlo (MC) method, density functional theory (DFT) and their combinations. All these methods are capable of modeling any problem associated with atomic motion, however, they are computationally demanding, as a consequence, limited to the number of atoms and to the time scale.

Comparably cost-effective method when dealing with large systems and longer durations is analytical continuum mechanics, which uses the theories of rods, beams, shells, trusses, or curved plates. This approach treats the lattice as continuous medium which in fact is discrete, and energies are obtained from analyzing the deformation of a plane graphene. Clearly, despite computational efficiency, its validity is questionable when applying to various problems: such assumptions neglect microscopic character of bonding as well as interatomic forces, thus ignoring microscopic effects on the mechanical response.

The third category, continuum mechanics based on FEMs uses finite elements such as rods, beams, springs to model atomic bonds. The method has become successful tool to learn elastic properties of CNTs.

Some of the representative studies related to shear modulus and fundamental band gap calculations under torsion are discussed below, both in chronological order.

Approaches to shear modulus calculations

Empirical force constant method used by Lu [30] has showed that elastic moduli of SWCNTs are insensitive to helicity and diameter; and that shear modulus is comparable to that of diamond. The nanotube geometry was obtained by mapping of the graphite sheet onto a cylindrical surface, while atomic interactions near equilibrium structure were represented as the sum of pairwise harmonic potentials; fitting parameters were determined by assuming equivalence of intraplane interactions in graphite and short-range atomic interactions in CNTs. Thus, parameters based on graphite calculations were employed. As an advantage of this method over MD simulations was considered its applicability to nanotubes of different size and type.

Popov *et al.* [51] deduced analytical expression for shear modulus using lattice-dynamics method by comparing expressions for the velocities of the torsional sound waves obtained through Born's perturbation technique and for the sound waves obtained from elasticity theory of infinite thin homogeneous cylinder. According to their calculations shear modulus for zigzag tubes was larger than that of armchair tubes for small radii, reaching converged value for bigger radii which was 6% smaller than that of graphite determined experimentally.

Structural mechanics approach has revealed that shear modulus of zigzag and armchair SWCNTs vary with the tube size, becomes independent of diameter above 2 nm and reaches the same value for zigzag and armchair nanotubes [29]. Within the investigated range of diameter (0.4-2.0 nm) no significant dependence on helicity was noted. In this approach assumption is that CNTs under load behave like space-frame structures and can be described with classical mechanics. Covalent bonds between carbon atoms are treated as connecting elements and carbon atoms are regarded as joints of them. Based on the same model and employing modified Morse potential similar results were obtained by Xiao *et al.* [60].

Based on the study utilizing FE approach, it was concluded that the shear moduli of zigzag, chiral and armchair SWCNTs depend on both, diameter and chirality, especially at diameters below 1.5 nm [50]. The dependence was explained as the effect of curvature, which in turn depends on the tube diameter. With the increase of diameter, shear moduli of all the tubes inclined to increase with the same trend and retained their value above d=1.1 nm.

Numerous modifications are made to improve the efficiency and accuracy of FE method:

According to To [49], FE modeling which treats SWCNTs as spatial cylindrical frame structures, is very simple to use, economical and computationally efficient. To's approach takes into account the effect of Poisson's ratio on the value of shear modulus. The study claims that shear modulus is independent of diameter.

Energy-equivalent model was first proposed by Odegard *et al.* [35] who combined computational chemistry and solid mechanics for simulating nanomaterials. The main

idea was equating the molecular potential energy and the strain energy of the continuum elements. In contrast to molecular modeling, it has been proved to be very efficient.

In a similar manner Wu *et al.* [59] calculated shear moduli of armchair and zigzag nanotubes by equating the total and strain energies found from molecular mechanics and continuum mechanics, respectively. Results demonstrated that shear modulus is sensitive to the diameter of the nanotubes. It was also shown that the value of the modulus approaches to that of graphite for large diameters.

Chandraseker *et al.* [10] compared an atomic-quasicontinuum method involving empirical Tersoff-Brenner interaction potential and *ab initio* DFT based on unit cell relaxations. In this study cylindrical reference configuration was assumed instead of planar graphene sheet what allows anisotropy and change in strain energy due to rolling up a graphene sheet into a nanotube. The work showed that the use of empirical interatomic potential in the quasicontinuum method results in the strong dependence of the outcome on the values of the fitted parameters, what reveals the unreliability of quasicontinuum approach. However, both methods agreed that the values of shear modulus were only slightly dependent on diameter as well as on chirality.

Giannopoulus *et al.* [22] introduced non-continuum FE method utilizing atomic microstructure of the nanotubes, where nodes were defined at carbon atom positions. Interatomic interactions were modeled by treating bonds as three-dimensional linear elastic spring elements having three rotational and three translational degrees of freedom. Thus, the study applies molecular mechanics directly and describes atomic bonds via force constants. Armchair nanotubes owned slightly lower values of shear modulus than zigzag nanotubes of the same diameter in case of small tubes. For large diameter tubes shear modulus converged to that of graphene as most of the studies indicate.

Atomistic-continuum modeling was introduced by Cheng *et al.* [12]. This model incorporates MD simulation for simulating initial unstrained equilibrium state, and finite element approximation for modeling static and dynamic behaviors. In this study surface effects on CNTs mechanical properties are taken into account as they are believed one of the main reasons of size dependence of material properties in nanostructures. In addition, they considered the influence of weak in-layer van der Waals interactions between atoms. The study revealed that shear modulus of zigzag and armchair nanotubes increases with increasing the diameter and above d=1.8 nm the value of shear modulus converges. Zigzag shear modulus was slightly larger than that of armchair, which means its dependence on chirality.

Most recent study has offered combination of molecular structural mechanics and finite element method which was aimed at developing a mechanical model for graphene, CNTs, buckypapers and their composites; and at determining their elastic moduli [62]. In the approach nanostructures are treated consisting of atoms as

structural masses or joints; chemical bonds and electrostatic forces are presented as mechanical elements (beams, trusses, springs). Since covalent bonds act linearly they are modeled with beam elements, on the contrary, van der Waals bonds are nonlinear and are therefore, modeled with nonlinear springs. Elastic moduli are obtained by linking the potential energy of bonds and the strain energy of mechanical elements similarly to reference 59. Bond energies and van der Waals bonds are calculated via harmonic and Lennard-Jones potentials, respectively. The outcome of the study is that shear modulus dependence on diameter is significant only for very small diameters.

Practical realization of twist of SWCNTs is problematic because of technical difficulties arisen from the size of nanomaterials; accordingly, there is indeed a lack of experimental data for describing twist in nanotubes. Among such rare studies is the realization of a torsional pendulum attached to a SWCNT [14]. Twisting was accomplished using an electric field. Torsional spring constant was evaluated from theory and device geometry and was found to be $3 \cdot 10^{-18}$ Nm per radian (for d=1.5 nm).

The first experimental measurement of the shear modulus of SWCNT was presented by Hall *et al.* [7]. They applied electrostatic forces to exert torsional stress on CNTs. The method was not novel but exploited different starting material than was used in earlier studies. Shear modulus was calculated within FE approximation by measuring the torque. The experiment demonstrated that SWCNT behaved as a linear torsional spring and average value of shear modulus approached 0.41 ± 0.36 TPa (for d=0.97 nm).

In summary, despite variations in the values of the elastic modulus and its dependency on chirality and tube diameter in different studies, the noted trend is that for large diameter CNTs shear modulus approaches that of graphene; disagreements appear at small sizes. This is on account of diverse assumptions, models, potentials, parameters, tube thicknesses and even different definitions of shear modulus used. That is why more reliable methods are needed for modeling specific nanostructures such as CNTs; and finding such an approach is still an ongoing process.

Studies about torsional behavior in the presence of vacancies are hardly to be found in literature. The only (to the best of our knowledge) study was carried out recently by Zhang *et al.* [65]. They performed molecular dynamics simulation to learn various kinds of defects including vacancies. The results showed that armchair CNTs had higher shear modulus and were less sensitive to the presence of defects compared to zigzag CNTs. It was noted that double vacancy diminishes torsional capacity more than single vacancy.

Excellent reviews on mechanical properties of CNTs are provided in references 49, 44, 60.

Approaches to fundamental band gap calculations

Not less attention is being paid to electronic properties of CNTs, especially to the band gap calculations. Band gap of SWCNTs changes under influence of electric and magnetic fields; and under mechanical strains [32].

Yet in 1999 Rochefort *et al.* [8] used Green's function technique and observed electronic band gap opening in (6,6) armchair nanotube during twist. Moreover, for constrained geometry gap increased linearly with increasing twisting angle, reached certain point and decreased linearly back to zero. Allowing relaxation in the twisted tubes resulted in saturation after reaching the maximum. For energy calculations they employed molecular mechanics approach and tight-binding DFT. Results showed that the energy needed for even moderate twist was very large. For small twists energy dependence on twisting angle was quadratic. In addition, structural relaxation was found to have a very strong effect on the deformation energy; the energy of the relaxed structure deviated from the quadratic law for large angles.

One of the most recent studies [32] suggested analytical derivation of the energy gap under small torsional strain within π-tight binding (π-TB) approximation. This method takes into account interactions of the nearest, the second and the third neighbors of each carbon atom, hence being sufficiently accurate. The study showed that the values of the band gaps in case of different chiralities change linearly with torsional strain. However, for different chiral vectors different levels and gradients in band gap change were observed, more precisely, if the remainder of $\frac{m-n}{3}$ was equal to 1, the gradient was negative, if -1, gradient was positive. In addition, greater radius resulted in greater shift in the band gap. Magnitude of the slope decreased with increasing the chiral angle. For bigger strains an abrupt change of the gradient sign was observed. This change was explained with interchanging of sub-bands that stand at the edges of conduction and valence bands.

Another recent study of torsion-induced band gap changes involving tight-binding calculations was carried out by Wang *et al.* [54]. They obtained analytical expression for energy gap of armchair and zigzag tubes using transfer matrix method. They represented a nanotube as a generalized honeycomb lattice on cylinder where straight line is replaced by a geodesic line and atomic positions are determined according to a cylindrical manifold, thus, taking into account curvature effects. Translation symmetry was realized using screw operation along tube axis. The method considers only nearest-neighbor hoppings for π-electrons modified by curvature effect and deformation. They observed linear relationship between the energy gap and twist for armchair nanotubes. In addition, it was noted that the energy gap corresponding to the same twist for smaller radius SWCNTs had smaller value. Chiral and zigzag tubes also revealed an increase with increasing twist. The small gaps were observed for pristine chiral and zigzag tubes which were predicted to be metallic according to tight-binding model of plain graphene described in section 1.2. Appearance of a gap in these tubes

is due to the curvature effect since it changes an overlap among π electron wavefunctions. Thus truly metallic are only armchair (m=n) CNTs and those, for which 1.4 condition is satisfied are semimetals with small energy gaps. The same was observed experimentally earlier [31].

Another approach for simulating torsions in CNTs is density functional tight-binding method (DFTB) combined with objective MD, which exploits helical symmetry instead of translational used in standard MD [16]. Energy band gap variation within this method had the same character as in above-mentioned studies: increasing linearly, reaching maximum halfway and, finally, decreasing to zero.

Chapter 3

Computational Methods

Since our work is performed within density-functional based tight-binding (DFTB) scheme, in this chapter we will first discuss both, density-functional theory (DFT) and its modification, DFTB. Afterwards we will overview symmetries related to SWCNTs which has a crucial role in the efficiency of our computations. In the last part of the chapter we will describe the two deformations we are interested in: shear, to be applied to graphene sheet, and torsion, to be applied to SWCNT.

3.1 Density-functional tight-binding method

DFTB scheme is the approximation of DFT obtained by parameterization [42]. It is our choice because of high computational speed and inherited accuracy. Moreover, its advantages over other schemes encompass reliability, transferability, independency of types of atoms, universality - it can be applied to ground state calculations to determine electronic structure as well as to excited state calculations to determine optical spectra in molecular systems. Before moving to DFTB we will briefly describe the many-body problem as an introduction to how it all began.

DFT: the origin of DFTB

Since 1990's the standard approach to many-body quantum mechanical problems has become density functional theory. DFT allowed to study much larger systems then it was possible within traditional *ab initio* methods and maintained the accuracy of its forerunner. The idea underlying DFT is to employ *functional*[*] of electron density instead of many-electron wave function. Hence, if earlier Schrödinger equation for N

[*]Functional by definition is mapping from vector space usually to the field of real numbers. If vector space is a space of functions, then functional can be explained as function of the function, returning scalar output. Square brackets are often used to denote inputs of the functionals.

electron system involved 3N variables, DFT reduced the problem to the only variable, the electron density.

General many-body Schrödinger equation involves kinetic energies of electrons and nuclei, electron-electron and nucleus-nucleus Coulumb interactions; and the potential acting on electrons exerted by nuclei. Obviously, such an equation is overly complicated to solve. An excellent, extremely useful approximation is Born-Oppenheimer (BO) approximation according to which nuclei, because of their big masses compared to electrons, can be treated as stationary (having fixed positions). Based on this assumption electron and nuclear parts of Schrödinger equation can be separated, *i.e.* many-body problem reduces to many-electron problem:

$$\hat{H}\Psi_j = E_j\Psi_j \tag{3.1}$$

where Ψ_j are many-electron wavefunctions, E_j eigenenergies of the system and $\hat{H}$ is a many-electron Hamiltionian consisting of four terms: kinetic term $\hat{T}$, electron-electron Coulomb interaction $\hat{V}_{ee}$, electron-nuclei interaction $\hat{V}_{e-nuclei}$ and electron interaction to external field $\hat{V}_f$[†]

$$\hat{H} = \hat{T}+\hat{V}_{ee}+\hat{V}_{e-nuclei}+\hat{V}_f = \underbrace{\sum_{i=1}^{N}\frac{1}{2}\nabla_i^2}_{\hat{T}} + \underbrace{\sum_{i\neq j}\frac{1}{|\boldsymbol{r}_i-\boldsymbol{r}_j|}}_{\hat{V}_{ee}} \underbrace{-\sum_{i=1}^{N}\sum_{m=1}^{M}\frac{Z_m}{|\boldsymbol{r}_i-\boldsymbol{R}_m|}+V_f}_{\hat{V}_{ext}} \tag{3.2}$$

Here, Z_m is the charge of nucleus m at position $\boldsymbol{R}_m$, $\boldsymbol{r}_i$ are positions of electrons, $\hat{V}_{ext}$ denotes the whole external potential on them.

Though BO approximation alleviated existing many-body problem, solving the many-electron Schrödinger equation was still enormously heavy task, especially for large systems.

Density functional theory revolutionized the many-body problem development. The starting point of DFT is Hohenberg-Kohn theorem which states that there exists unique correspondence between the ground state electron density $n_0(\boldsymbol{r})$, the electron wavefunction Ψ and the external potential V_{ext} [38]. Moreover, electron density uniquely defines all the ground state observables of the system through the wavefunction. In one word, once the ground state electron density is known, all the ground state properties of a system are known.

Then total energy within DFT is given by the following expression:

$$E[n] = F[n] + V_{ext}[n] = T[n] + V_{ee}[n] + \int n(r)\left(-\sum_m \frac{Z_m}{|\boldsymbol{r}_i-\boldsymbol{R}_m|}+V_f\right)dr \tag{3.3}$$

[†]Equations are written in atomic units, *i.e.* $e = \hbar = m_e = 1$.

As ground state energy means the lowest available energy for the system, applying variational principle and minimizing expression (3.3) with respect to electron density gives the ground state electron density n_0 and ground state energy $E[n_0] \equiv E_0$. Nonetheless, this procedure is again cumbersome. Therefore, approximations had to be made. Soon after appearing Hohenberg-Kohn theorem, W. Kohn and L. J. Sham suggested the scheme that simplifies the variational principle routine for interacting electrons in external potential [57]. Based on Hellman-Feynman theorem [‡] they introduced the model system of non-interacting fictitious electrons in effective (single-particle) external potential whose many-body wavefunction yields the same electron density as the original interacting-electron system, hence, the two systems having identical ground state densities:

$$\left(-\frac{1}{2}\nabla^2 + v_s[n](\boldsymbol{r})\right)\phi_i(\boldsymbol{r}) = \epsilon_i\phi_i(\boldsymbol{r}) \tag{3.4}$$

$$n(\boldsymbol{r}) = \sum_i |\phi_i(\boldsymbol{r})| \tag{3.5}$$

where, $v_s[n]$ is a single particle potential functional and is represented as the sum of the external potential $v_{ext}[n]$, the potential due to all-electron density $v_{ee}[n]$ and the potential that can be referred as correction in order to take into account many-body effects (exchange-correlation) $v_{xc}[n]$:

$$v_s[n](\boldsymbol{r}) = v_{ext}[n] + v_{ee}[n] + v_{xc}[n] \tag{3.6}$$

Equations (3.4)-(3.6) are termed Kohn-Sham equations. They require self-consistent solution; That is, calculations start with initial guess for ground state density and corresponding Kohn-Sham potential v_s is found. According to new v_s, new density is calculated and the routine repeats until convergence in electron density and potential is reached.

Forces acting on atoms, as a consequence of Helmann-Feynmann theorem, can be calculated as the derivative of Hamiltonian with respect to nuclear coordinates. Finally, KS equations transform many-electron problem to single-particle problem. More detailed discussions on DFT can be found in references 52, 9, 37.

[‡]Hellmann-Feynman theorem relates the derivative of total energy with respect to parameter λ to the expectation value of the derivative of Hamiltonian with respect to the same parameter: $\frac{\partial E}{\partial \lambda} = \int \psi^*(\lambda)\frac{\partial \hat{H}_\lambda}{\partial \lambda \psi(\lambda)}d\tau$. The outcome of the theorem is that if electron distribution is known, forces can be determined through the principles of classical electrostatics.

Tight-binding formalism of DFTB

Without going into details we will focus on the main points of DFTB. More detailed derivation of DFTB and the examples of applications are given, for instance, in references 21 and 40.

DFTB scheme starts with representing KS orbitals Ψ_a of the system for eigenstate a as the linear combination of atomic orbitals ϕ_ν:

$$\Psi_a(r) = \sum_\nu c_{a\nu}\phi_\nu(\boldsymbol{r}). \tag{3.7}$$

In other words, DFTB uses minimal basis set, *i.e* to each angular momentum state only one radial function corresponds. In case of translationally periodic lattices equation (3.7) can be rewritten using Bloch's waves:

$$\Psi_{a,\mu}(\boldsymbol{k},\boldsymbol{r}) = \frac{1}{\sqrt{N}}\sum_{\boldsymbol{T}} exp(i\boldsymbol{k}\cdot\boldsymbol{T})\phi_\mu(\boldsymbol{r}-\boldsymbol{T}) \tag{3.8}$$

where $\boldsymbol{T}$ describes the translation periodicity of the lattice and ϕ_μ are atom-centered localized basis functions. Using such basis total energy of DFT expressed with equation (3.3) transforms to DFTB total energy:

$$E_{DFTB} = E_{BS} + E_{Coulumb} + E_{rep} \tag{3.9}$$

where the first term is the band-structure energy, the energy with neutral electron density and without charge transfer in Hamiltonian. The second term represents the energy due to charge fluctuations which contains in itself mainly Coulomb interaction and exchange-correlation. The third term is repulsive energy for the pair of atoms, which is fitted to certain reference systems and is parametrized using DFT.

Minimizing E_{DFTB} via variational principle, KS equations transform to a set of algebraic equations:

$$\sum_v c_{a\nu}(H_{\mu\nu} - \epsilon_a S_{\mu\nu}) = 0 \quad \forall\mu, a \tag{3.10}$$

$$H_{\mu\nu} = H^0_{\mu\nu} + \frac{1}{2}S_{\mu\nu}\sum_K(\gamma_{IK}+\gamma_{KJ})\Delta q_K, \quad \mu\in I, \nu\in J \tag{3.11}$$

where $H^0_{\mu\nu} =< \phi_\mu|H^0|\phi_\nu >$ are matrix elements of Hamiltionian which in tight-binding approach are parameters (numbers). $S_{\mu\nu}$ represent overlap matrix elements; Δq_K is excess charge on atom K and $\gamma_{IK}(\gamma_{LJ})$ describes Coulomb interaction between atoms I and K (L and J).

As it is seen from equations (3.10) and (3.11), overlap is not generally zero, $S_{\mu,\nu} = < \phi_\mu|\phi_\nu > \neq \delta_{\nu\mu}$. Calculating overlap integral is based on numerical integration of Slater-Koster integrals. Obtained values are stored in a table only once for all orbital

pairs. Then, by interpolation overlap can be obtained for any geometry. $H_{\mu\nu}$ are computed in two-center approximation. This means that only nearest neighbors are taken into consideration. Hamiltonian matrix elements are parametrized directly from DFT, similarly to $S_{\mu\nu}$. Thus, avoiding heavy calculations of integrals at each step as it is done in DFT.

Equations (3.10) and (3.11) need to be solved self-consistently alike standard DFT: calculations start with initial guess for Δq_K according to which $H_{\mu\nu}$ is found. Next, from equations (3.10) new $c_{a\nu}$ is obtained which gives new value for Δq_K. Iterations repeat until convergence is reached.

Forces can again be found by taking gradients of E_{DFTB} with respect to atomic positions.

To summarize, in DFTB total energy of the system is composed of three terms: band structure, repulsive and Coulomb energies, each dependent on atom pairs and their separations only. Matrix elements and repulsive potentials are derived from DFT. Due to pre-parameterization, DFTB is a few orders faster than DFT without sacrificing accuracy too much.

3.2 Symmetries of carbon nanotubes

Whatever the high performance computer is used existing today, simulating large systems is still limited by the insufficiency of computational resources. It is doubtful if technology would ever be possible to remove these limits unless certain novel approach from the side of theory is made. The way to reduction of computational costs (thus increasing the limiting size of the system) goes through symmetries. [§]From quantum-mechanical point of view this means that the wavefunction must be invariant with respect to symmetry operation.

For instance, well-known Bloch's theorem allows to simulate translation-periodic systems using a *unit cell* containing only a few atoms: within such a symmetry the solutions of the Schrödinger equation can be represented as the product of the plane wave $exp(i \cdot \boldsymbol{k})$ and the function $u_{\boldsymbol{k}}$ having the lattice periodicity: [¶]

$$\psi_{\boldsymbol{k}}(\boldsymbol{r}) = u_{\boldsymbol{k}}(\boldsymbol{r}) exp(i \cdot \boldsymbol{r}) \tag{3.12}$$

where $\boldsymbol{k}$ is the wavevector. Thus, thanks to Bloch's theorem instead of considering the whole system, only one cell can be analyzed to find the function $u_{\boldsymbol{k}(\boldsymbol{r})}$; next, by modulating with plane wave, wavefunction of the whole system can be determined.

[§]Symmetry, in terms of molecules means that upon atomic permutations the system returns to the state indistinguishable from the initial. Such an operation is termed symmetry operation.

[¶]Discussion on Bloch's theorem can be found in any solid state physics textbooks, for example, in reference [27].

Figure 3.1 illustrates how three-dimensional translation-periodic system can be generated using a single simulation cell described with the three translational vectors $\boldsymbol{T}_1$, $\boldsymbol{T}_2$ and $\boldsymbol{T}_3$.

Despite all, translational periodicity is not always the best choice, especially in case of cylindrical and helical systems, such as nanotubes, DNA helix, nanotori, bent, twisted nanomaterials. For example, translational unit cell of (10,9) helical nanotube would contain 1084 carbon atoms [15], obviously, even this small nanotube requires huge computational resources. Hence, the challenge is to find the smallest unrepeatable unit of the system which using symmetry transformations and imposing proper boundary conditions will produce information (wavefunction) about the whole system.

With this goal White *et al.* [15] were the first to use helical and rotational symmetries instead of translational in their tight-binding calculations of the band gaps for semiconducting CNTs. They introduced the construction of a nanotube by initially mapping only two atoms on the surface of the cylinder and next, applying the two symmetry operations as depicted in figure 3.2.

The two-atom mapping was further used by Popov [41] for calculating electronic band structure and the dielectric function of small- and moderate-radius SWCNTs using symmetry-adapted non-orthogonal tight-binding scheme. Non-translational symmetries were used also by Zhang and Dumitrica [63] for investigating elastic properties of relaxed and distorted CNTs.

How exactly can this be exploited in computations? If Bloch's theorem simplifies calculations for the bulk owning translational symmetry, it is logical to predict that there must exist similar deductions for the systems with other types of symmetries; Thus, to state once again, the way to accomplishment is to first find the smallest unit cell which via symmetry operations will construct the entire system; next, to perform all the calculations within this unit cell; finally, to make symmetry-based implications

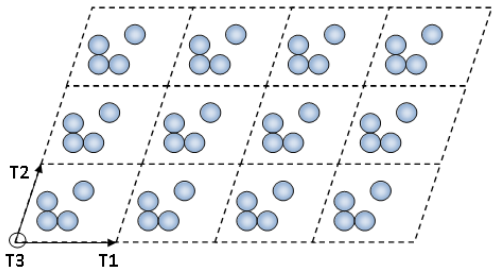

Figure 3.1: Generating translation-periodic system using simulation cell defined with vectors $\boldsymbol{T}_1$, $\boldsymbol{T}_2$ and $\boldsymbol{T}_3$ ($\boldsymbol{T}_3$ perpendicular to the sheet plane).

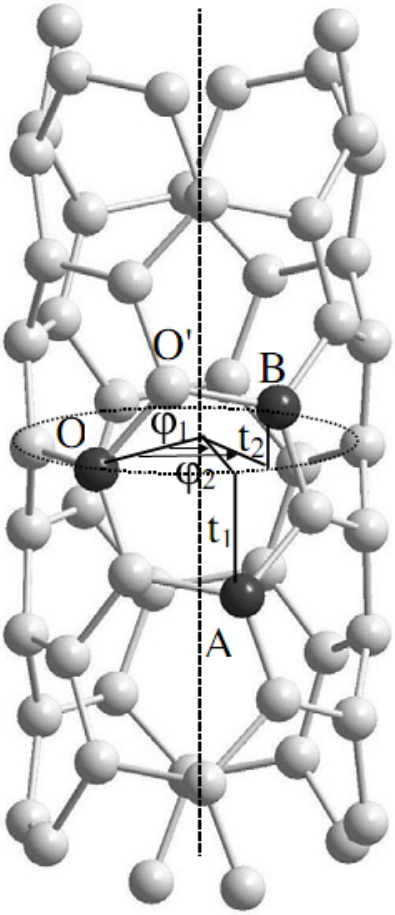

Figure 3.2: Mapping a pair of atoms on a cylindrical surface for generating nanotube. Atom O turns into atom A via rotation by angle ϕ_1 around the tube axis and translation at distance t_1. Analogously, atom O coincides with atom B for the screw operation described with ϕ_2 and t_2. Picture is taken from reference 41.

to predict the wavefunction of the entire system.

Generalized Bloch's Theorem

Recently, Koskinen and Kit [39] introduced revised Bloch's theorem valid for any system which is invariant under translation and/or rotations:

> *In a potential, that is invariant in symmetry operations S^n, the energy eigenstates $\psi_{a\boldsymbol{\kappa}}$ at $\boldsymbol{r}$ and at $\boldsymbol{r}' = S^{-\boldsymbol{n}}\boldsymbol{r}$ differ by a phase factor $exp(i\boldsymbol{\kappa}\cdot\boldsymbol{n})$*

$$\hat{D}(S^n)\psi_{a\boldsymbol{\kappa}}(\boldsymbol{r}) = \psi_{a\boldsymbol{\kappa}}(S^{-n}\boldsymbol{r}) = exp(i\boldsymbol{\kappa}\cdot\boldsymbol{n})\psi_{a\boldsymbol{\kappa}}(\boldsymbol{r}) \tag{3.13}$$

Where $\hat{D}(S^n)$ is the invariant transformation of the potential: $\hat{D}(S^n)V(\boldsymbol{r}) = V(S^{-n}) = V(\boldsymbol{r})$; $S^n = S_1^{n_1}S_2^{n_2}...$, $S_i(i = 1, 2, ...)$ being any symmetry operation(s) (translation, rotation, reflection and their combinations) and n=$(n_1, n_2, ...)$.S^{-n} is the inverse transformation of S^n. $\psi_{a\boldsymbol{\kappa}}(\vec{r})$ with $\boldsymbol{\kappa} = (\kappa_1, \kappa_2, ...)$ are eigenstates of both, $\hat{D}(S^n)$ and $\hat{H}$ as the two operators commute due to invariance.

Equation (3.13) entails that the wavefunction of a single unit cell determine the electronic structure of the whole system, regardless of the shape of the unit cell. It is analogous to the Bloch's theorem with the difference that in Hamiltonian and overlap matrix elements instead of k points κ (kappa) points appear, which is the result of additional symmetries. Consequently, this is the only difference between the two total energy expressions and high symmetry points k now become κ. To sum up, revised Bloch's theorem is generalization of well-known Bloch's theorem beyond translational symmetry and is the way to more efficient computations for distorted materials.

Unit cell of the system

In the remaining part of the section we will discuss simulation cell setups for cylindrical and helical systems.

The two main coordinate transformations of our interest are rotation and translation:

Rotation operation $\mathcal{R}_{\alpha_n}$ rotates $\boldsymbol{r}$ with angle α around the axis circumscribed by the vector $\boldsymbol{\alpha}_n$ so that $\boldsymbol{r}$ appears into $\boldsymbol{n}$th image[‖]:

$$\boldsymbol{r}_n \equiv \mathcal{R}_{\alpha_n}\boldsymbol{r} \tag{3.14}$$

and

$$\begin{cases} \boldsymbol{\alpha}_n = n\boldsymbol{\alpha} \\ \boldsymbol{n} = (n, 0, 0) \end{cases} \tag{3.15}$$

[‖]Image is termed the cell obtained by symmetry transformations of the simulation cell.

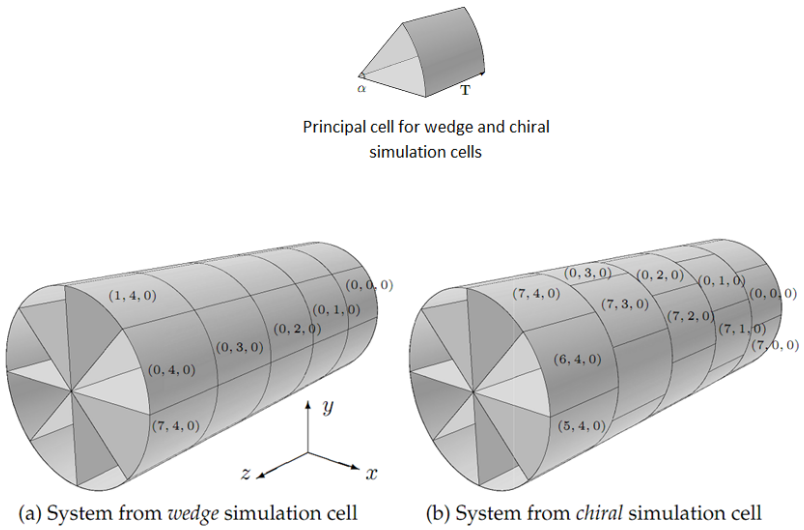

Figure 3.3: Simulation cells generated from the principal cells described with angle α and vector $\boldsymbol{T}$. $\boldsymbol{n} = (n_1, n_2, 0)$ numerate the images of the principal cell $\boldsymbol{n} = (0, 0, 0)$. Figure is taken from reference 26.

Such transformations generate simulation cell for 2D periodic systems characterized with the only parameter $\boldsymbol{\alpha}$. The simulation cell is termed *wedge simulation cell* with *wedge angle* α [26].

Translation operation $\mathcal{T}_T$ means displacement of $\boldsymbol{r}$ with the given vector $\boldsymbol{T}$:

$$\boldsymbol{r}_n \equiv \mathcal{T}_T \boldsymbol{r} = \boldsymbol{r} + \boldsymbol{T} \tag{3.16}$$

Depending on the combinations of rotations and 1D translations, either cylindrical or helical nanostructures can be generated: The sequence of operations

$$\begin{cases} \boldsymbol{\alpha}_n = n_1 \boldsymbol{\alpha} \\ \boldsymbol{T}_n = n_2 \boldsymbol{T} \qquad \boldsymbol{\alpha} \| \boldsymbol{T} \\ \boldsymbol{n} = (n_1, n_2, 0) \end{cases} \tag{3.17}$$

produce a system with cylindrical symmetry (figure 3.3a). Here, rotation and translation are made independently. While either

$$\begin{cases} \boldsymbol{\alpha}_n = n \boldsymbol{\chi} \\ \boldsymbol{T}_n = n \boldsymbol{T} \qquad \boldsymbol{\chi} \| \boldsymbol{T} \\ \boldsymbol{n} = (n, 0, 0) \end{cases} \tag{3.18}$$

or

$$\begin{cases} \boldsymbol{\alpha}_n = n_1\boldsymbol{\chi}_1 + n_2\boldsymbol{\chi}_2 \\ \boldsymbol{T}_n = n_1\boldsymbol{T}_1 + n_2\boldsymbol{T}_2 \quad \boldsymbol{\chi}_1\|\boldsymbol{\chi}_2\|\boldsymbol{T} \\ \boldsymbol{n} = (n, 0, 0) \end{cases} \tag{3.19}$$

that is, coupled combinations of rotation and translation, generate helical systems and the simulation cell is called *chiral simulation cell* (figure 3.3b).

More rigorous discussion on wedge and chiral simulation cell setups can be found in reference 26.

3.3 Shear and torsion of plane and thin cylindrical elastic objects

When atoms are displaced in a solid by external force, an opposite, restoring force is induced which tries to return them in their equilibrium positions. Small deformations are usually *elastic*, *i.e.* able to fully recover initial positions of the distorted atoms after removing load. Our study is carried out within elastic range, therefore, we will only consider this limiting case.

Elastic response of material is characterized with two basic quantities: *stress*, defined as force per unit area and *strain*, a quantity characterizing the amount of deformation that object experiences under stress compared to its initial geometry. Classical approach is based on Hook's law stating that stress is proportional to strain. The constant of proportionality is called elastic modulus. One can interpret it as a measure of material's ability to resist mechanical load.

Depending on the type of deformation there exist three main moduli of elasticity [48]:

Young's modulus Y, describing tensile deformation and characterizing resistance of a solid to uniaxial stretching (figure 3.4 a)). *Bulk modulus* K, characterizing hydrostatic compression (figure 3.4 b)). *Shear modulus* G, describing resistance of a material to shear deformation (figure 3.4 c)). Our subject of interest is shear modulus. As it is seen shear means stress acting parallel to the surface which changes angles but preserves the volume of a sample (or area in 2D which is our case). Shear deformation is characterized with *shear constant* γ_s:

$$\gamma_s = \tan\theta = \frac{\Delta x}{h} \tag{3.20}$$

where Δx is displacement and h is the distance between the sheared edges (figure 3.5). For small deformations $tan\theta \approx \theta$.

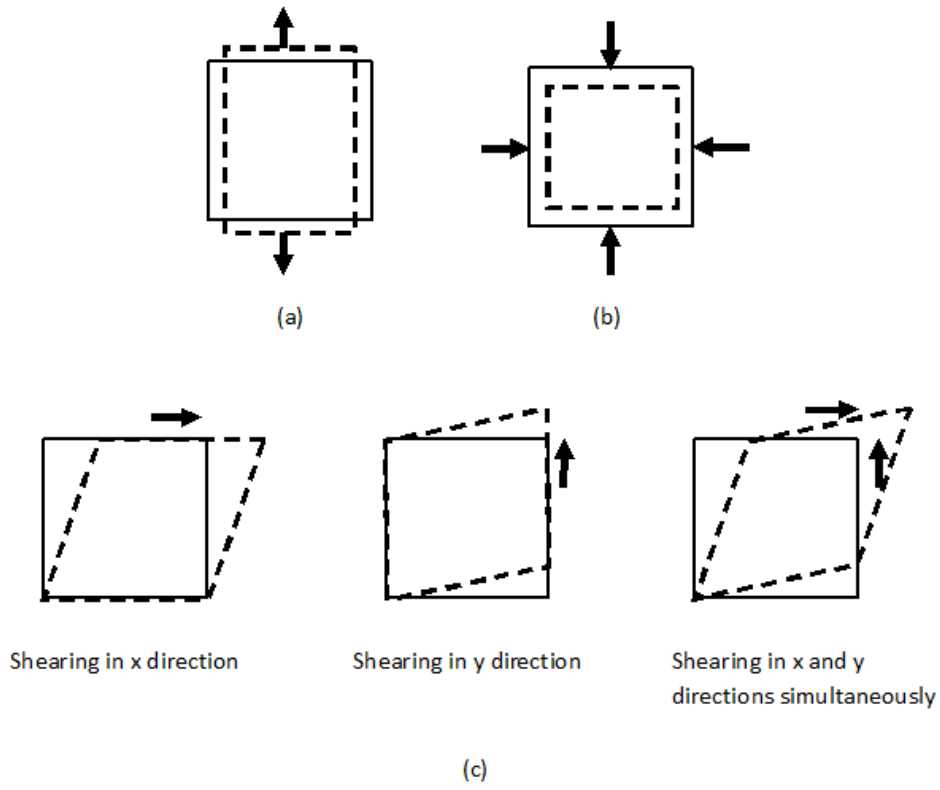

Figure 3.4: Three types of elastic deformations: (a) tensile, (b) hydrostatic compression, (c) shear. They are characterized with Young's modulus Y, Bulk modulus K and Shear modulus G, respectively. Arrows indicate the direction of the applied force.

When considering cylindrical objects, *torsion* (termed also as uniaxial twist, or simply, twist) can be understood as relative rotation of the two ends in opposite directions around the tube axis, usually, one end is assumed to be fixed while the other is rotated. Such kind of deformation is described with *torsion constant*:

$$\gamma_t = \frac{r\phi}{h} \tag{3.21}$$

where r is the radius of the cylinder, ϕ, the twisting angle, and h is the height of the sample (figure 3.6).

Continuum mechanics relates shear modulus of a material to the torsion constant

Figure 3.5: Shear characterized with angle θ: $tan\theta = \frac{\Delta x}{h}$.

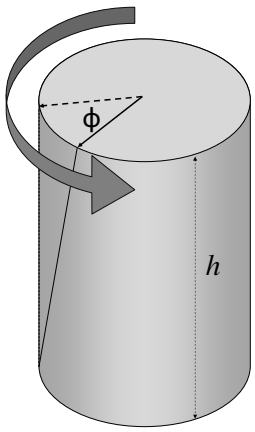

Figure 3.6: Twist of a cylinder with hight h characterized with angle ϕ.

via energy of the sample:

$$G = \frac{1}{V}\frac{\delta^2 E}{\delta\gamma^2}, \tag{3.22}$$

where V is the volume of the object.

3.4 Hotbit and Atomic Simulation Environment

`Hotbit` is a calculator for python module Atomic Simulation Environment (ASE) with implemented DFTB code and generalized symmetries [1, 40, 28]. DFTB makes

computations faster, while properly chosen symmetries help to significantly reduce the number of atoms in a simulation cell.

`Hotbit` gives opportunity to model distorted nanomaterials with wedge and chiral symmetries. Chiral simulation cell is used to generate carbon nanotubes and continuous twist on them (as twist itself owns chiral symmetry).

Chapter 4

Results and Discussion

The reason why we are interested in the two particular deformations is the assumption that twisting carbon nanotube becomes equivalent to shearing graphene sheet when the tube diameter approaches infinity. We calculate shear moduli for both using equation (3.22).

For small twists energy dependence on torsion obeys quadratic law [8]: $E = C\gamma^2 + B\gamma + E_0$, where C and B are constants. B is small enough to be negligible, corresponding to the assumption of perfectly isotropic lattice of graphene. Thus, equation (3.22) becomes

$$G = \frac{2C}{V}. \tag{4.1}$$

Our general scheme for finding values of G is as follows: After initial optimization, first we calculate total energies during torsion in the range $\gamma \in (-0.1, 0.1)$ with step 0.005, and with $\gamma \in (0, 0.1)$ when torsion effect is the same in opposite directions; next, we find coefficient C from $E - \gamma$ curve using quadratic fit, finally, we define G from equation (4.1). Similar procedure is carried out for shearing graphene.

Volumes are treated as volumes of a parallelepiped and that of a hollow cylinder for graphene and nanotubes, respectively. We take the reference thickness t of these two nanostructures to be equal to 3.4 Å, however, its value has no particular importance in our calculations: as we are comparing shear moduli of graphene and those of nanotubes, relative quantitative relationship between them would be the same for arbitrarily chosen t. In fact, thickness of an one-atom layer nanostructure even lacks physical sense.

It must be emphasized that we consider continuum mechanics only for the definition of shear modulus which requires finite dimensions (equation (3.22)); since shear and twist deformations characterize bulk, we treat graphene and nanotube as bulk, having fixed volume, with the sole purpose to define shear and twist on them. Otherwise, as the origin of deformation is intrinsically microscopic, we choose to calculate energies, needed to determine shear modulus, and forces, needed for optimization,

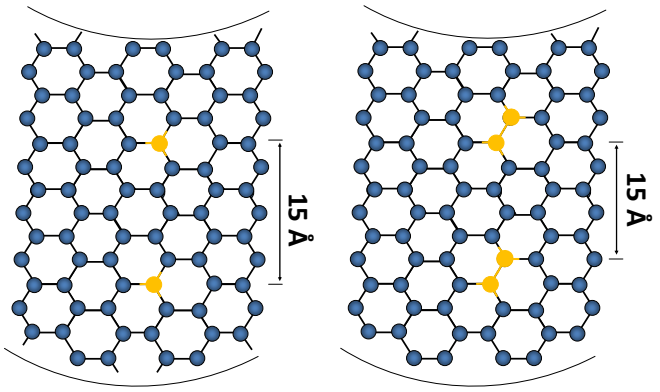

Figure 4.1: Single(a) and double(b) vacancies in carbon nanotubes aligned with the tube axis.

quantum mechanically, using DFTB scheme as mentioned in the previous chapter. Optimization is done via Broyden–Fletcher–Goldfarb–Shanno (BFGS) method.

In addition to pristine case, we perform studies on nanotubes with point defects: single and double vacancies. Defects are situated along the tube axis with a distance of approximately 15 Å between them as illustrated in figure 4.1.

Studies involve three sets of SWCNTs: (5,0), (10,0) and (15,0) zigzag tubes, (3,3), (6,6) and (9,9) armchair tubes, and (4,2), (7,5) and (10,8) chiral tubes. In order to observe chirality and diameter effect during torsion, nanotubes are chosen in a way that $d(5,0) \approx d(3,3) \approx d(4,2) = d1$, $d(10,0) \approx d(6,6) \approx d(7,5) = d2$, and $d(15,0) \approx d(9,9) \approx d(10,8) = d3$, where d stands for the diameter of the tube.

In the following part of the chapter performed computational study will be presented. The work consists of four main parts: i) Determination of shear modulus behavior under twist for perfect SWCNTs and comparison to that of graphene. ii) Determination of shear modulus behavior under twist in the presence of point defects, single vacancy (SV) and double vacancy (DV) cases. iii) Investigating shear modulus dependence on shearing direction for pristine graphene, also for graphene with SV and DV. iv) Finding electronic fundamental gap response to twist for perfect tubes.

Each problem is described and analyzed separately in the four sections of the chapter preceding our expectations for the outcome. Obtained results are compared to the information found in literature.

Chirality	(n,m)	$d1$	G_{d1}	(n,m)	$d2$	G_{d2}	(n,m)	$d3$	G_{d3}
Zigzag	(5,0)	0.39	0.491	(10,0)	0.78	0.509	(15,0)	1.17	0.509
Armchair	(3,3)	0.41	0.432	(6,6)	0.81	0.509	(9,9)	1.22	0.516
Chiral	(4,2)	0.41	0.474	(7,5)	0.82	0.485	(10,8)	1.22	0.499

Table 4.1: Obtained shear moduli for pristine nanotubes. Gs are given in units of TPa and diameters in nm.

4.1 Shear modulus calculations for perfect SWCNTs

CNT properties can not be straightforwardly concluded based on graphene because of curvature effect present in the tube. Obviously, behavior of the curved surface can not be identified with that of flat sheet. Moreover, the smaller the tube diameter, the bigger the curvature and the stronger the effect is. Our assumption is that torsion should become equivalent to shearing graphene for large diameters. Figure 4.2 shows computational results for pristine tubes. As it is seen, result agrees with our expectations: shear moduli of all the nanotubes gradually approach that of graphene as diameter increases, regardless of chirality.

At small diameters picture is different, G is dependent on chirality: armchair nanotube has the smallest elastic modulus which turns out to be the most sensitive to size, while shear modulus of zigzag nanotubes seem to be less dependent on diameter and is higher than that of the other two tubes. This is in agreement with references 51 and 22, where zigzag tubes were reported to have the highest shear modulus at small diameters. Convergence of shear moduli was confirmed in most of the studies, for example, in reference 29 it was reached at d=2 nm, in reference 50 - at d=1.1 nm, in reference 12 - at d=1.8 nm. According to our results convergence is reached at $d \approx$1.2 nm, however, deducing exact limit from our studies would not be reasonable at this point - significantly large data has to be investigated then. Computed values of G are presented in table 4.1.

4.2 Shear modulus calculations in the presence of single- and double vacancies.

As we have studied how deformation alters elastic properties of pure nanotubes, it is important to check what kind of behavior would deformation together with point defect exhibit. Vacancy is a missing atom from lattice site, this makes structure less rigid than in perfect case, therefore, we expect that shear modulus for single vacancy

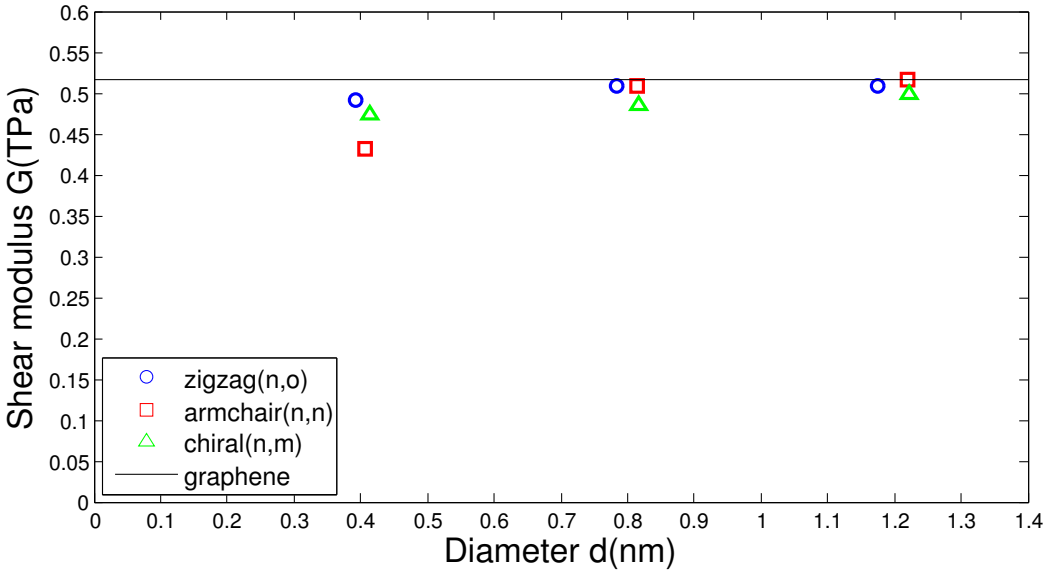

Figure 4.2: Shear moduli of perfect SWCNTs and graphene. Graphene shear modulus corresponds to shearing zigzag graphene sheet and is 0.517 TPa; Shearing in armchair direction results in the value of 0.515 TPa which is not shown here to avoid overloading the figure.

Chirality	(n,m)	$d1$	G_{d1}	(n,m)	$d2$	G_{d2}	(n,m)	$d3$	G_{d3}
Zigzag	(5,0)	0.39	0.489	(10,0)	0.78	0.487	(15,0)	1.17	0.506
Armchair	(3,3)	0.41	0.440	(6,6)	0.81	0.497	(9,9)	1.22	0.509
Chiral	(4,2)	0.41	0.471	(7,5)	0.82	0.497	(10,8)	1.22	0.509

Table 4.2: Obtained shear moduli for the nanotubes with single vacancy. Gs are given in units of TPa and diameters in nm.

must be diminished compared to pristine tubes, double vacancy is supposed to provide even smaller moduli. In addition, we anticipate that G must increase with diameter: since we are studying all the nanotubes with the same number of vacancies, for small diameters vacancy concentration is bigger than for the larger ones. Figure 4.3 and table 4.2 show obtained results for single vacancy case and corresponding numerical values. Shear moduli increases with diameter especially for armchair tubes, however, as in the case of pristine tubes zigzag nanotubes are almost independent of diameter,

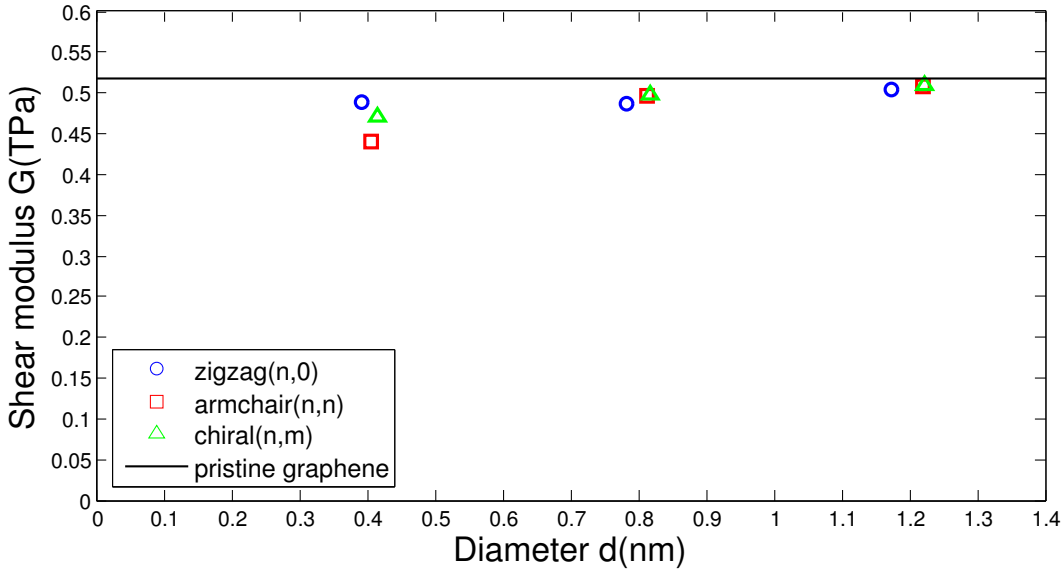

Figure 4.3: Shear moduli of armchair, zigzag and chiral SWCNTs with single vacancy.

Chirality	(n,m)	$d1$	G_{d1}	(n,m)	$d2$	G_{d2}	(n,m)	$d3$	G_{d3}
Zigzag	(5,0)	0.39	0.483	(10,0)	0.78	0.488	(15,0)	1.17	0.512
Armchair	(3,3)	0.41	0.443	(6,6)	0.81	0.487	(9,9)	1.22	0.502
Chiral	(4,2)	0.41	0.450	(7,5)	0.82	0.483	(10,8)	1.22	0.502

Table 4.3: Obtained shear moduli for the nanotubes with double vacancy. Gs are given in units of TPa and diameters in nm.

only slight change in G is observed. When compared to pure case, zigzag nanotubes have decreased shear modulus for all sizes, armchair tubes show increase in G as well as larger chiral tubes, thus no clear picture of the trend can be established about armchair and chiral ones, which might be the outcome of small torsions. Zhang *et al.* [65] also reported that armchair nanotubes where less sensitive to the presence of defects than zigzag tubes.

Results for double vacancy and the values of G are shown in figure 4.4 and table 4.4, respectively. Here, chiral tubes show absolute decrease in modulus, and no strict trend is noted for the other two types, however, decrease occurs in most of the tubes, though the smallest armchair and larger zigzag tubes exhibit opposite.

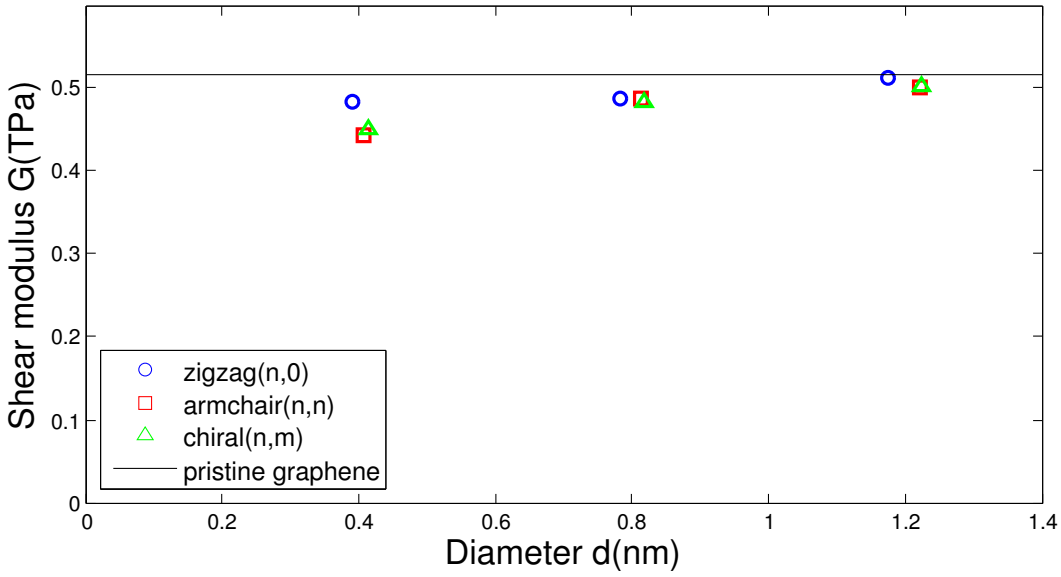

Figure 4.4: Shear moduli of armchair, zigzag and chiral SWCNTs with double vacancy.

Fixed separation between the point defects implies that the vacancy concentration in the tubes of unequal diameter will be different: the smaller the tube, the less percent of atoms are missing and the less rigid material is; Figures 4.5a and 4.5b depict that regardless of chirality and the tube diameter shear moduli decreases almost linearly with the increase of vacancy percentage. Linear approximation is particularly good for small vacancy concentrations, below 1% for SV and below 2% for DV.

The trend slope is noted to be smaller for a pair-vacancy than that of single vacancy, what predicts that nanotubes are more stable against the number of DVs.

4.3 Shear modulus response to the shearing direction of graphene

Changing shearing direction of a graphene sheet corresponds to changing chirality of a twisted tube. We describe it with angle α between x axis and the direction of applied force. For example, shearing in x direction ($\alpha = 0$) in our study is equivalent to twisting zigzag tube, consequently, shearing in y($\alpha = \pi/2$) direction corresponds to twisting armchair tube. All other directions correspond to twisting chiral tubes. Figure 4.6a presents calculations in the range $\alpha \in (0, \pi/2)$. This range fully characterizes

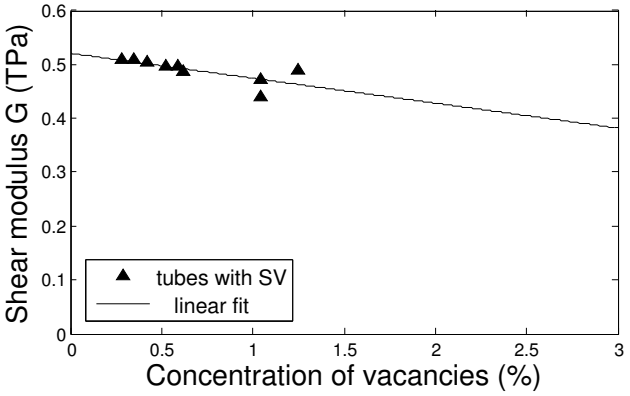

(a)

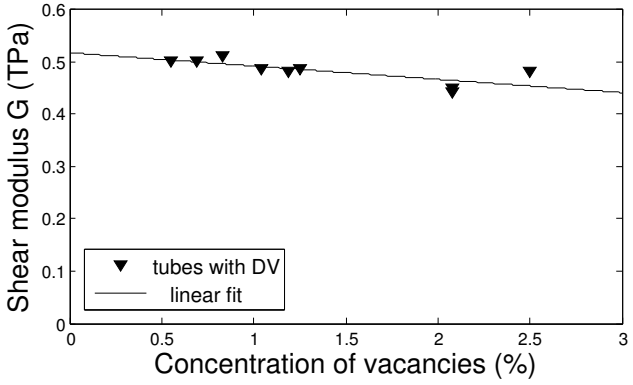

(b)

Figure 4.5: Shear modulus change with single(a) and double(b) vacancy concentration.

shearing in any direction because of symmetry of a pristine graphene. Maximum deviation from the average value G_{av}=0.516 TPa is 1.16% and occures at maximum and minimum values of G reached.

In case of single vacancy fluctuations are minor as found from figure 4.6b, from minimum value - 0.4% and from maximum - 0.2%. This indicates at only slight dependence on chirality of shear modulus in case of SV, which is also seen from figure 4.3 for larger diameter tubes.

Double vacancy causes more fluctuations as depicted in figure 4.6c. Here, deviations from minimum and maximum are 1.7% and 3.2%, respectively, which are highest compared to the above two cases. Accordingly, we can predict that DV is most sensitive to chirality at shear deformation for large tubes.

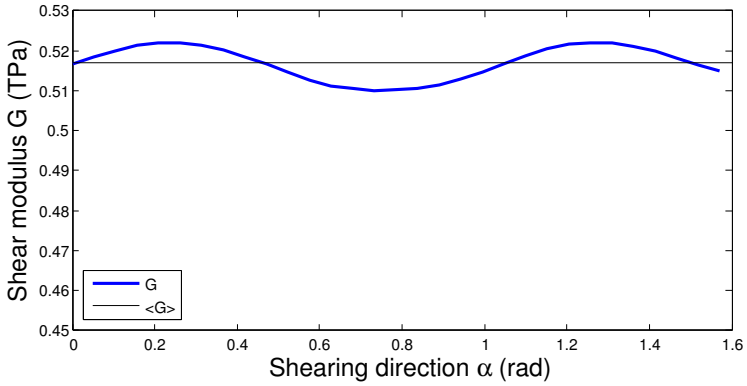

(a) perfect graphene

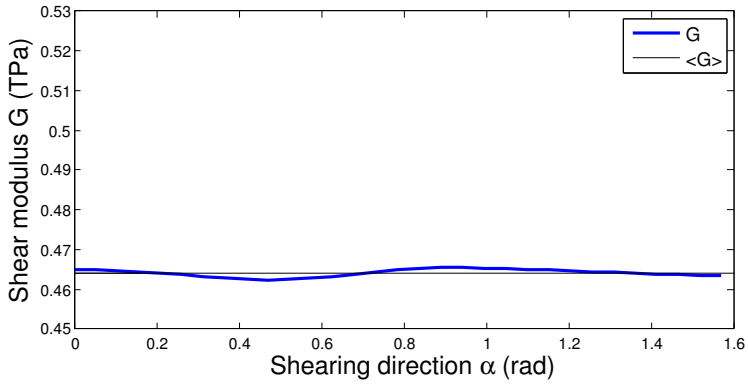

(b) graphene with SV

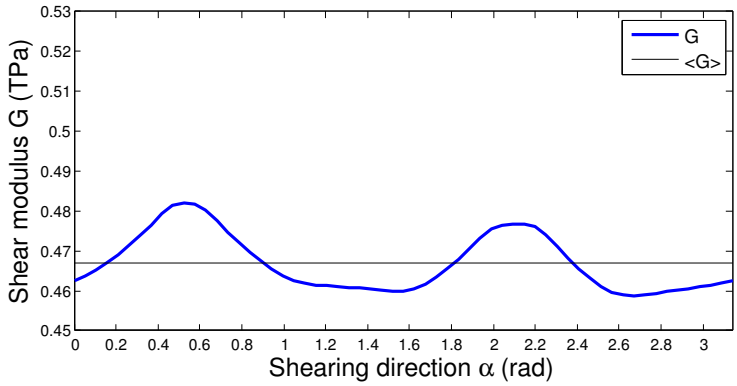

(c) graphene with DV

Figure 4.6: Shear modulus variation depending on the shearing direction of perfect(a) graphene and in the presence of single(b)- and double(c) vacancies. DV graphene shows most sensitivity to shearing direction.

Case	G_{min}(TPa)	G_{max}(TPa)	G_{av}(TPa)
Pristine	0.510	0.522	0.516
SV	0.462	0.465	0.464
DV	0.459	0.482	0.467

Table 4.4: Interesting values of shear modulus for direction-dependent shearing of graphene.

4.4 Finding electronic fundamental gap response to twist for perfect tubes

Deformation modifies not only elastic properties of a material but also electronic. Bond distortion affects electronic structure, consequently, band gap variation is expected. It is already known that armchair nanotubes experience metal to semiconductor transition during torsion [8],[16]. In this part of the work we investigate the effect of twist on the energy gap for our sets of SWCNTs. We estimate band gap from Density of States (DOS) calculations at each step of the deformation in the same interval of torsion as above.

Metallic zigzag tubes (5,0)* and (15,0) did not exhibit any significant change in DOS near Fermi level and remained metallic in the whole range of torsion, while E_{gap} of semiconducting (10,0) tube fluctuates with torsion as shown in figure 4.7a. Critical point where increase starts is at $\gamma = 0.02$.

On the contrary, all armchair tubes maintain metallic behavior only until $\gamma = 0.03$, which is followed by linear increase in E_{gap} with almost the same slope for all the tubes, reaching maximum, and decreasing linearly for (3,3) and (9,9) as figure 4.7b depicts. Linearity can be explained with the tight-binding band structure of graphene, for which dispersion relation near Fermi energy is linear due to the degeneracy of the bands as presented in figure 4.8.

Chiral nanotubes behave similarly to armchair ones as seen from figure 4.7c, except that the gap opening starts at negative values of torsion reminding about their specific achiral symmetry.

The values of maximum gaps $E_{\Delta gap}$ reached for the tubes from zigzag and chiral groups, corresponding to the same diameter, come closer as the tube diameter increases, *i.e.* $E_{\Delta gap}$=0.32 eV of (10,8) and $E_{\Delta gap}$=0.33 eV of (9,9) are closest compared to the other two pairs, while $E_{\Delta gap}$=0.61 eV of (4,2) and $E_{\Delta gap}$=0.42 eV have the highest difference. Above discussion is visualized in figure 4.9. This raises the supposition that for large diameter tubes the maximum energy gap reached during torsion should converge.

*It must be noted that in opposite to simple tight-binding model which predicts (5,0) to be semiconducting (equation 1.4), DFTB reveals its metallic character caused by the small diameter.

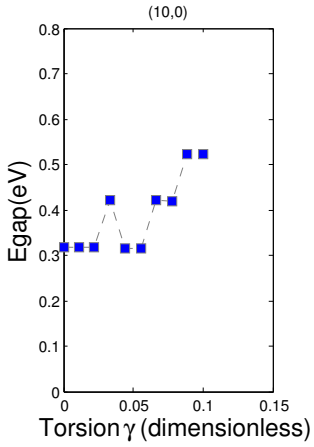

(a) zigzag

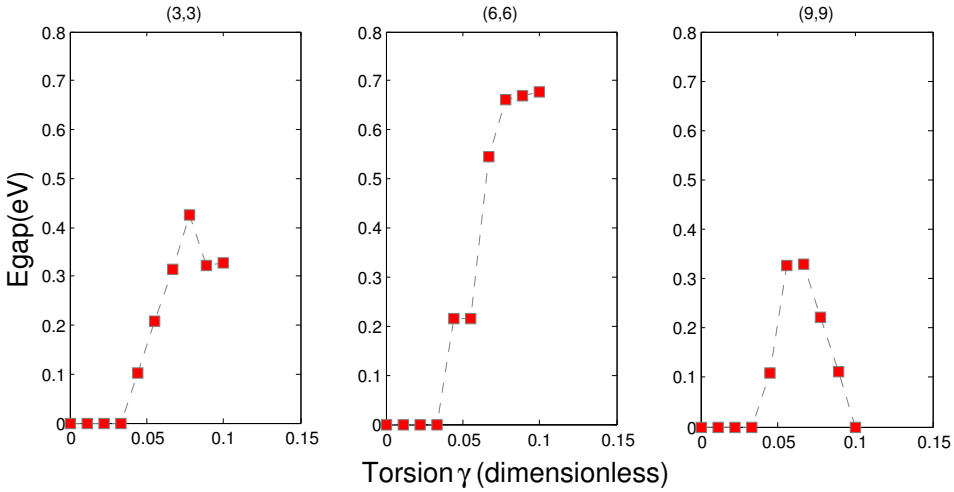

(b) armchair

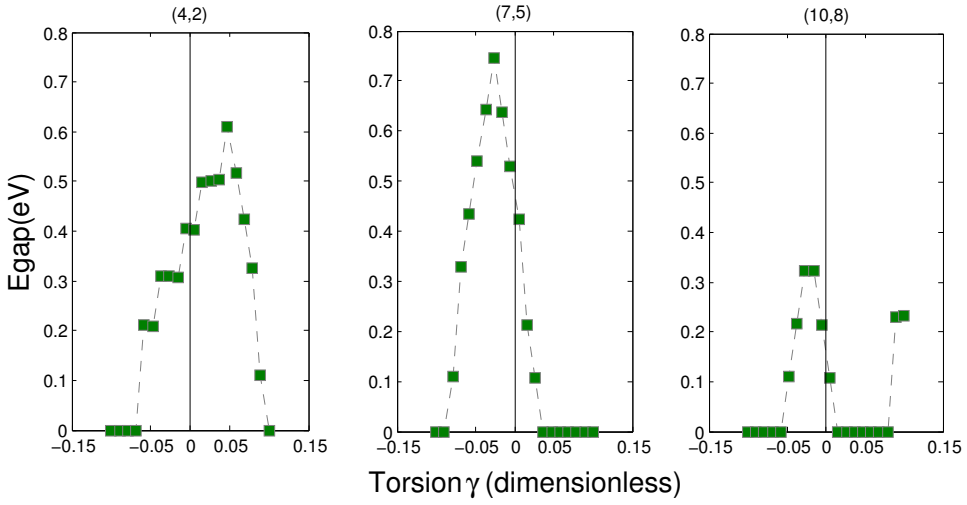

(c) chiral

Figure 4.7: Energy gap response to torsion for zigzag, armchair and chiral nanotubes.

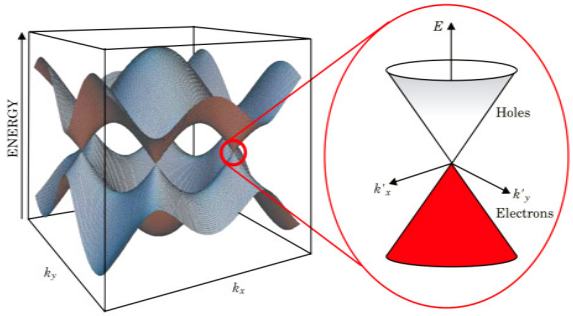

Figure 4.8: Electronic band structure of graphene: degeneracy of conduction and valence bands result in the linear relation between energy E and wave vector $\boldsymbol{k}$ in the vicinity of Fermi level. Fermi level passes through the points where the two bands meet.

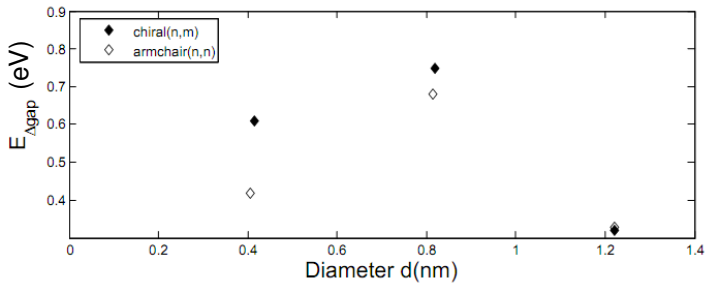

Figure 4.9: The difference between the torsion-induced fundamental gap values disappears with the increase of diameter for the same size of tubes with different chirality.

The figure also illustrates that biggest tubes exhibit smallest gaps which is the case in metallic pristine tubes as well [56]. However, no gap-diameter correlation was found in our study due the insufficient size of data.

The slope of the increase (decrease) of E_{gap} in figure 4.7 according to simple tight-binding model of graphene is equal to $3t_0 r$, where t_0 is the tight-binding hopping element and r is the radius of the nanotube. Zhang *et al.* [16] found good agreement between tight-binding prediction and DFTB calculations for cylinder idealized shape of (12,12) nanotube. They found t_0=2.72 eV which is close to 2.66 eV used by Yang *et al.*. However, our study offers different results for the vales of hopping parameter than mentioned above and deviates between 0.6-1.6 eV. Disagreements could be evoked by the small range of torsion used in our studies where finer disturbances in electronic structure are observed, and where simple tight-binding approach can not be applied.

Chapter 5

Summary and outlook

The main part of the thesis embraces literature review and performed computational work. The first chapter includes the general discussion on carbon nanotubes and their properties and explains the motivation for CNT research.

Chapter 2 overviews existing methods and results related to the thesis topic. The need for further studies is inferred and emphasized; seeking the perfect way for modeling mechanical and electronic properties of CNTs is still an ongoing process, despite the number of methods attempted. This is implied by the variations in shear modulus calculation results and by the lack of studies of simultaneously distorted and point-defected tubes.

Our approach to modeling deformed carbon nanotubes and the fulfilled work are given in chapters 3 and 4, respectively. Symmetry-adapted Density-Functional Tight-Binding method makes calculations fast without sacrificing accuracy. Therefore, we consider it ideally suitable for performing studies on twisted carbon nanotubes.

Results for shear modulus calculations mostly agree with literature, namely, as tube diameter increases its value becomes equal to that of graphene independently of chirality, confirming that the properties of large diameter tubes can be explained based on flat graphene. However, this is not the case at small diameters: armchair carbon nanotubes exhibit the smallest shear modulus and are most sensitive to size compared to their zigzag and chiral counterparts. On the other hand, zigzag tubes have the highest modulus at small diameters and are least sensitive to size. However, in the presence of vacancies armchair nanotubes had no any significant change in moduli. General picture is that SV decreases shear modulus for most of the tubes, DV even more. Shear modulus dependence on concentration of vacancies was also studied. The outcome is linear decrease with the percentage of point defects, regardless of chirality. As a future work, it would be interesting to conduct more detailed work on larger data and to establish more solid relationship between the vacancy concentration and shear moduli. This would give possibility to identify the presence of point defects according to the known shear modulus for the known size of the tube.

Chirality dependence is more rigorously studied by shearing the graphene sheet in different directions, covering the whole characteristic range. The most sensitive to direction variations was found graphene with DV, associating with nanotubes, this predicts that tubes with DV must be most sensitive to chirality at large diameters.

The effect of torsion on electronic properties is expressed by inducing the electronic band gap in initially metallic nanotubes. The changing character is linear, reaching maximum at certain point. Results suggest that for large tubes the peak values of opened band gaps must be the same for all affected tubes. The study could be further extended to learn the band gap change in graphene under shear. Point-defect effect on band gap of twisted nanotubes would also remain as future challenge.

In summary, the current thesis is an effort to get insight into torsional behavior of SWCNTs. Once the defect related behavior is firmly resolved the way to tuning nanotube properties via imperfections is opened, and better control of nanotube based devices is possible. However, to achieve complete controllability there is yet much to learn.

Bibliography

[1] Atomic Simulation Environment. `https://wiki.fysik.dtu.dk/ase/`, October 2010.

[2] Epitaxial graphene on silicon carbide. `http://www.andrew.cmu.edu/user/feenstra/graphene/`, October 2010.

[3] European technology innovation award for hyptonite. `https://www.jyu.fi/en/news/archive/2010/02/tiedote-2010-02-26-13-58-20-380667`, February 2010.

[4] The official web site of the Nobel Prize. `http://nobelprize.org/nobel_prizes/physics/laureates/2010/info.html`, October 2010.

[5] University of Wisconsin, materials research science and engineering center. `http://www.mresc.wisc.edu/Edetc/nanoquest/carbon/index.html`, June 2010.

[6] A.K.Geim and K.S.Novoselov. The rise of graphene. *Nature*, 6, 2007.

[7] A.R.Hall, L.An, J.Liu, L.Vicci, M.R.Falvo, R.Superfine, and S.Washburn. Experimental measurement of single-walled carbon nanotube torsional properties. *Physical Review Letters*, 96(25):256102, 2006.

[8] A.Rochefort, P.Avouris, F.Lesage, and D.R.Salahub. Electrical and mechanical properties of distorted carbon nanotubes. *Physical Review B*, 60(19):13824–13830, 1999.

[9] K. Capelle. A bird's-eye view of density-functional theory. *arXiv:cond-mat/0211443v5 [cond-mat.mtrl-sci]*, 2006.

[10] K. Chandraseker and S. Mukherjee. Atomistic-continuum and *ab initio* estimation of the elastic moduli of single-walled carbon nanotubes. *Computational materials science*, 40:147–158, 2007.

[11] J.C. Charlier, X. Blase, and S.Roche. Helical microtubules of graphitic carbon. *Reviews of Modern Physics*, 79(2):677–732, 2007.

[12] H.C. Cheng, Y.L. Liu, Y.C. Hsu, and W.H. Chen. Atomistic-continuum modeling for mechanical properties of single-walled carbon nanotubes. *International Journal of Solids and Structures*, 46:1695–1704, 2009.

[13] C.Liu, Y.Y.Fan, M.Liu, H.T.Cong, H.M.Cheng, and M.S.Dresselhaus. Hydrogen storage in single-walled carbon nanotubes at room temperature. *Science*, 286(5442):1127–1129, 1999.

[14] J. C.Meyer, M. Paillet, and S. Roth. Single-molecule torsional pendulum. *Science*, 309(5740):1539–1541, 2005.

[15] C.T.White, D.H. Robertson, and J.W. Mintmire. Helical and rotational symmetries of nanoscale graphicitc tubules. *Physical Reveiw B*, 47(9):5485–5488, 1993.

[16] D.B.Zhang, R.D.James, and T.Dumitrica. Electromechanical characterization of carbon nanotubes in torsion via symmetry adapted tight-binding objective molecular dynamics. *Physical Review B*, 80(11):115418, 2009.

[17] Alan B.Dalton *et al.* Continuous carbon nanotube composite fibers:properties,potential applications, and problems. *Journal of Materials Chemistry*, 14:1–3, 2004.

[18] Morinobu Endo, Takuaya Hayashi, Yoon Ahm Kim, Mauricio Terrones, and Milred S.Dresselhaus. Applications of carbon nanotubes in the twenty-first century. *Phil. Trans. R. Soc. Lond. A*, 362(1823):2223–2238, 2004.

[19] Erik.T.Thostenson, Zhifeng Ren, and Tsu-Wei Chou. Advances in the science and technology of carbon nanotubes and their composites: a review. *Composites Science and Technology*, 61:1899–1912, 2001.

[20] D.S. Chung et al. Carbon nanotube electron emitters with a gated structure using backside exposure processes. *Applied Physics Letters*, 80(21):4045–4047, 2002.

[21] T. Frauenheim, G. Seifert, M. Elstner, et al. Atomistic simulation os complex materials: ground-state and excited-state properties. *Journal of Physics: Condensed Matter*, 14(11):3015–3047, 2002.

[22] G.I. Giannopoulos, P.A.Kakavas, and N.K. Anifantis. Evaluation of the effective mechanical properties of single walled carbon nanotubes using a spring based finite element approach. *Computational Materials Science*, 41:561–569, 2008.

[23] J. H. Hafner, C. L. Cheung, A. T. Woolley, and C. M. Lieber. Structural and functional imaging with carbon nanotube AFM probes. *Progress in Biophysics and Molecular Biology*, 77(1):73–110, 2001.

[24] Ray H.Baughman. Playing nature's game with artificial muscles. *Science*, 308(5718):63–65, 2005.

[25] J.Bernholc, D.Brenner, M.Buongiorno Nardelli, V.Meunier, and C.Roland. Mechanical and electrical properties of nanotubes. *Annual Review of Material Research*, 32(1):347–375, 2002.

[26] O.O. Kit. Generalized symmetries in nanostructure simulations. Master's thesis, University of Jyväsklyä, 2009.

[27] Charles Kittel. *Introduction to Solid State Physics*. Wiley, 2004.

[28] P. Koskinen. DFTB calculator for ase. `https://trac.cc.jyu.fi/projects/hotbit/`, October 2010.

[29] Chunyu Li and Tsu-Wei Chou. A structural mechanics approach for the analysis of carbon nanotubes. *International Journal of Solids and Structures*, 40(10):2487–2499, 2003.

[30] J.P. Lu. Elastic properties of carbon nanotubes and nanoropes. *Physical Review Letters*, 79(7):1297–1300, 1997.

[31] M.Ouyang, J.L. Huang, C.L. Cheung, and C.M. Lieber. Energy gaps in.

[32] M.Pakkhesal and R.Ghayour. Mechanically changed band gap of single walled carbon nanotube: a thirt neighbor tight-binding approach. *Central European Journal of Physics*, 8(3):304–311, 2010.

[33] N.Hamada, S.Sawada, and A.Oshiyama. New one-dimensional conductors: Graphitic microtubules. *Physical Review Letters*, 68(10):1579–1581, 1992.

[34] O.Breuer and Uttandaraman Sundararaj. Big returns from small fibers: A review of polymer/carbon nanotube composites. *Polymer Composites*, 25:630–645, 2004.

[35] G.M. Odegard, T.S. Gates, M.Nicholson, and E. Wise. Equivalent-continuum modeling of nano-structured materials. *Composites Science and Technology*, 62(14):1869–1880, 2002.

[36] P.Avouris, Z.Chen, and V.Perebeinos. Carbon-based electronics. *Nature Nanotechnology*, 2:605–615, 2007.

[37] J.P. Perdew and S.Kurth. *Density Functionals for Non-Relativistic Coulomb Systems*. 1998.

[38] P.Hohenberg and W.Kohn. Inhomogenous electron gas. *Physical Review*, 136(3B):B864–B871, 1964.

[39] P.Koskinen and O.O. Kit. Efficient approach for simulating distorted materials. *Physical Review Letters*, 105(10):106401, 2010.

[40] P.Koskinen and V.Mäkinen. Density-functional tight-binding for beginners. *Computational Materials Science*, 47:237–253, 2009.

[41] V.N. Popov. Curvature effects on the structural, electronic and optical properties of isolated single-walled carbon nanotubes within a symmetry-adapted non-orthogonal tight-binding model. *New Journal of Physics*, 6:17, 2004.

[42] D. Porezag, Th. Frauenheim, Th. Köhler, G.Seifert, and R.Kaschner. Construction of tight-binding-like potentials on the basis of density-functional theory:application to carbon. *Physical Review B*, 51(19):12947–12957, 1995.

[43] R.Saito, M.Fujita, G.Dresselhaus, and M.S. Dresselhaus. Electronic structure of chiral graphene tubules. *Applied physics letters*, 60:2204–2206, 1992.

[44] M.M Shokrieh and R.Rafiee. A review of the mechanical properties of isolated carbon nanotubes and carbon nanotube composites. *Mechanics of Composite Materials*, 46(2):155–172, 2010.

[45] S.Iijima. Helical microtubules of graphitic carbon. *Nature*, 354(7):56–58, 1991.

[46] S.Iijima and T. Ichihashi. Single-shell carbon nanotubes of 1-nm diameter. *Nature*, 363(17):603–605, 1993.

[47] T. Spires and Jr. R.Malcolm Brown. High resolution TEM observations of single-walled carbon nanotubes, August 1996.

[48] William S.Slaughter. *The Linearized Theory of Elasticity*. Birkhäuser Boston, 2001.

[49] C.W.S. To. Bending and shear moduli of single-walled carbon nanotubes. *Finite Elements in Analysis and Design*, 42:404–413, 200.

[50] K.I Tserpes and P.Papanikos. Finite element modeling of single-walled carbon nanotubes. *Composites Part B: Engineering*, 36:468–477, 2005.

[51] V.N.Popov and V.E. Van Doren. Elastic properties of single-walled carbon nanotubes. *Physical Reveiw B*, 61:3078–3084, 2000.

[52] U. von Barth. Basic density-functional theory-an overview. *Physica Scripta*, 2004(T109):9, 2004.

[53] Q.H. Wang, M.Yan, and R.P.H. Chang. Flat panel display prototype using gated carbon nanotube field emitters. *Applied Physics Letters*, 78:1294–1296, 2001.

[54] S. Wang, R.Wang, X.Wu, H.Zhang, and R.Liu. Axial strain and twist-induced changes in the electronic structure of carbon nanotubes. *Physica E*, 42:2250–2256, 2010.

[55] Xueshen Wang, Qunqing Li, Jing Xie, Zhong Jin, Jinyong Wang, Yan Li, Kaili Jiang, and Shoushan Fan. Fabrication of ultralong and electrically uniform single-walled carbon nanotubes on clean substrates. *Nano Letters*, 9(9):3137–3141, 2009.

[56] J.W.G Wildöer, L.C. Venema, A.G.Rinzler, R.E. Smalley, and C. Dekker. Electronic structure of atomically resolved carbon nanotubes. *Nature*, 391(1):59–62, 1998.

[57] W.Kohn and L.J.Sham. Self-consistent equations including exchange and correlation effects. *Physical review*, 140(4A):A1133–A1138, 1965.

[58] W.Krätschmer, L.D.Lamb, K.Fostiropoulos, and D.R.Huffman. Solid c60: a new form of carbon. *Nature*, 347:354–358, 1990.

[59] Y. Wu, X. Zhang, A.Y.T.Leung, and W. Zhong. An energy-equivalent model on studying the mechanical properties of single-walled carbon nanotubes. *Thin-Walled Structures*, 44:667–676, 2006.

[60] J.R. Xiao, B.A. Gama, J.W. Gillespie, and Jr. An analytical molecular structural mechanics model for the mechanical properties of carbon nanotubes. *International Journal of Solids and Structures*, 42(11-12):3075 – 3092, 2005.

[61] Min-Feng Yu, Oleg Lourie, Mark J. Dyer, Katerina Moloni, Thomas F. Kelly, , and Rodney S. Ruoff. Strength and breaking mechanism of multiwalled carbon nanotubes under tensile load. *Science*, 287(5453):637–640, 2000.

[62] M.M. Zaeri, S. Ziaei-Rad, A. Vahedi, and F. Karimzadeh. Mechanical modelling of carbon nanomaterials from nanotubes to buckypaper. *Carbon*, 48:3916–3930, 2010.

[63] D.B. Zhang and T.Dumitrica. Elasticity of ideal single-walled carbon nanotubes vis symmetry-adapted tight-binding objective modeling. *Applied Physics Letters*, 93:031919–1, 2008.

[64] Wei-De Zhang and Wen-Hui Zhang. Carbon nanotubes as active components for gas sensors. *Journal of Sensors*, 2009:16 pages, 2009.

[65] Y.Y. Zhang, C.M. Wang, and Y. Xiang. A molecular dynamics investigation of the torsional responses of defective single-walled carbon nanotubes. *Carbon*, 48(14):4100–4108, 2010.